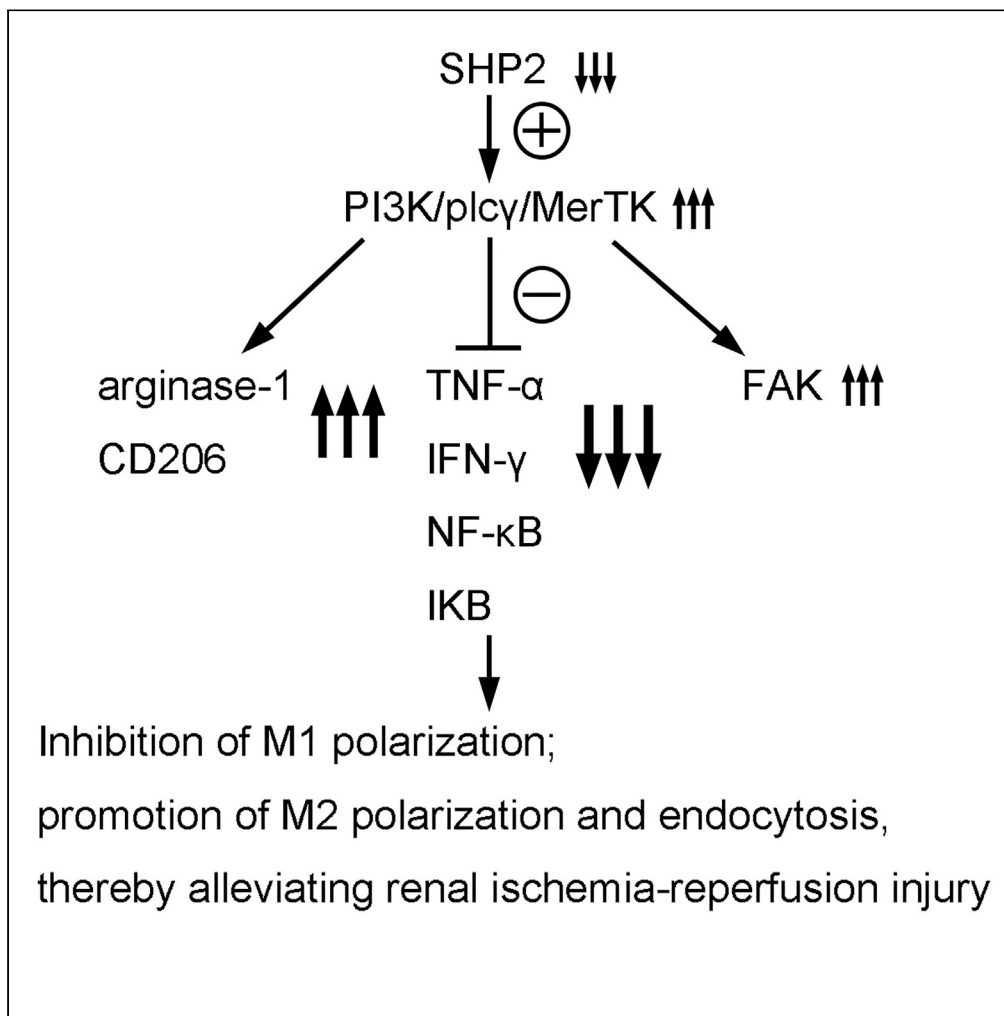


Article

Specific knockout of macrophage SHP2 promotes macrophage M2 polarization and alleviates renal ischemia-reperfusion injury



Meilian Du,
Shanbao Zhang,
Xiaoyu Wang,
Chen Liu, Linrong
Pan, Xiao Chen,
Yinghui Qi

shali8416@163.com

Highlights

To investigate the effect of specific macrophage knockout SHP2 on renal IRI

Inhibition of SHP2 promotes endocytosis in macrophages

Inhibition of SHP2 can promote the PI3K/PLCγ/MerTK signaling pathway

Inhibition of SHP2 can reduce inflammation and damage caused by renal IRI

Article

Specific knockout of macrophage SHP2 promotes macrophage M2 polarization and alleviates renal ischemia-reperfusion injury

Meilian Du,¹ Shanbao Zhang,¹ Xiaoyu Wang,¹ Chen Liu,¹ Linrong Pan,¹ Xiao Chen,¹ and Yinghui Qi^{1,2,*}

SUMMARY

To investigate the effect of specific knockout of SHP2 in mononuclear macrophages on renal ischemia-reperfusion injury and its molecular mechanism. The structural, functional, and pathological changes in the mouse kidney were detected by ultrasound testing. The relative fluorescence intensity of α -SMA, Col1, Col3, and Vim was measured by immunofluorescence staining, and ELISA was performed to detect the concentrations of blood urea nitrogen (BUN), creatinine (Crea), and uric acid (UA). The relative protein expressions of relevant proteins in the mouse kidney tissue were detected by western blotting. Specific knockout of SHP2 could improve both renal function and structure, reduce the relative fluorescence intensity of α -SMA, Col1, Col3 and Vim, lower the concentrations of BUN, Crea, and UA and the expressions of TNF- α , IFN γ , p-NF κ B, and p-MyD88, and increase the expressions of p-MerTK, p-FAK, p-PI3K, and p-I κ B. The above results illustrate that specific knockdown of macrophage SHP2 promotes macrophage M2 polarization and alleviates renal ischemia-reperfusion injury. The above results illustrate that specific knockdown of macrophage SHP2 promotes macrophage M2 polarization and attenuates renal ischemia-reperfusion injury. Specific knockout of macrophage SHP2 promotes macrophage M2 polarization and alleviates renal ischemia-reperfusion injury.

INTRODUCTION

Renal ischemia-reperfusion injury (IRI) is defined as a restriction in the organ blood supply, followed by restoration of blood flow and reoxygenation causing injury. The infarction, sepsis, and organ transplantation are often accompanied by subsequent unavoidable injury, which worsens the damage of tissues by inducing an inflammatory cascade involving reactive oxygen species (ROS), cytokines, chemokines, and leukocyte activation.^{1,2} Acute kidney injury (AKI), a clinical condition characterized by rapid renal failure and high mortality, can be brought on by IRI. The pathophysiology of IRI is incredibly complex and involves several pathological pathways such as release of ROS and activation of neutrophils and other inflammatory mediators including adhesion molecules and multiple cytokines.³⁻⁵

Inflammation, a frequent manifestation of IRI, appears to play a crucial role in connecting various cell types and is a key component of IRI pathophysiology. Inhibiting inflammatory response is a strategy to protect kidney tissues since IRI can trigger an inflammatory cascade that results in severe kidney damage. Chemokines regulate the expressions of pro-inflammatory cytokines and adhesion molecules as well as the infiltration and activation of leukocytes, thereby serving as primary mediators of inflammation. In IRI, pro-inflammatory cytokines and other cytokines such as interleukin-6 (IL-6) and tumor necrosis factor- α (TNF- α) are vital factors.^{6,7} Macrophages, depending on the cytokines that stimulate them or the microenvironments they are exposed to, can differentiate into various phenotypes. Pro-inflammatory cytokines such as IL-1, TNF- α , and IL-6 are expressed when M1 macrophages are exposed to interferon (IFN), lipopolysaccharide (LPS), TNF, or granulocyte-macrophage colony-stimulating factor (GM-CSF), while M2 macrophages stimulated by IL-2/IL-4 can produce anti-inflammatory cytokines, including IL-10 and TGF- β .⁸ Studies have demonstrated that renal tubular epithelial cells produce macrophage growth factors like M-CSF, GM-CSF, and IL-34, which are involved in the activation and polarization of macrophages. Macrophages can activate and upregulate the CD206 and arginase-1 expressions when co-cultured with renal tubular epithelial cells.^{9,10} Based on the aforementioned findings, it can be inferred that macrophages can alleviate renal IRI and promote subsequent recovery. Phosphatidylinositol 3-hydroxy kinase (PI3K)/protein kinase B (Akt) is an important signaling pathway that regulates metabolism, growth, migration and proliferation of various cells. PI3K is capable of phosphorylating the 3'-hydroxyl group of the inositol ring of phosphatidylinositol. Prior research has demonstrated the beneficial effects of PI3K/Akt activation against IRI, with such mechanisms as inhibiting cell apoptosis, reducing ROS generation, and restraining inflammatory responses.^{11,12}

Src homology 2 (SH2) domain-containing tyrosine phosphatase-2 (SHP2), a non-receptor tyrosine phosphatase, is encoded by the PTPN11 gene. SHP2 was the first phosphatase to be identified as a human oncoprotein, which is closely related to Noonan syndrome, Leopard skin syndrome, and juvenile myelomonocytic leukemia. SHP2 protein consists of one protein phosphatase catalytic domain at the C terminal and

¹Department of Nephrology, Pudong New District Punan Hospital, Shanghai 200125, China

²Lead contact

*Correspondence: shali8416@163.com

<https://doi.org/10.1016/j.isci.2024.109048>



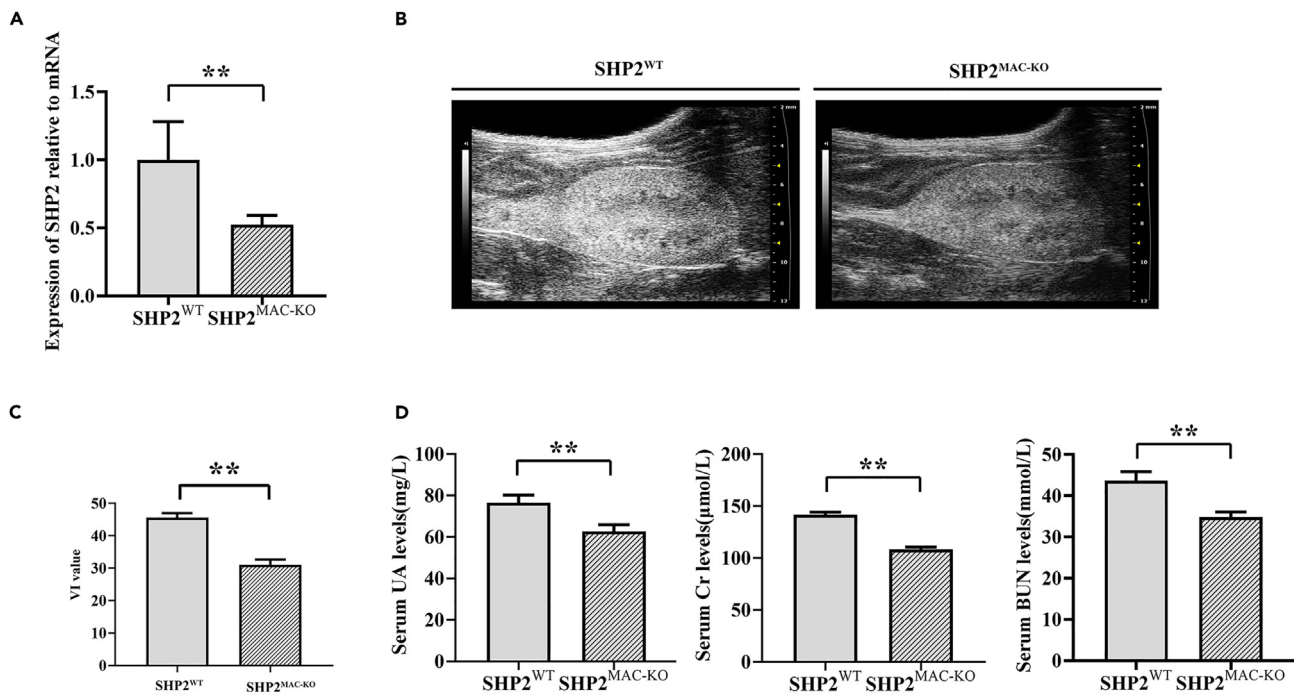


Figure 1. Renal ultrasound results in SHP2^{WT} group and SHP2^{MAC-KO} group
 (A) RT-PCR detected SHP2 expression in the SHP2^{WT} group and the SHP2^{MAC-KO} group.
 (B) Ultrasound image of kidney in SHP2^{WT} group and SHP2^{MAC-KO} group.
 (C) VI value of kidney in SHP2^{WT} group and SHP2^{MAC-KO} group.
 (D) Chart of ELISA results. N = 8; **p < 0.01.

two SH2 domains at the N terminal (C-SH2 and N-SH2). N-SH2 is considered to be a conformational switch. The overall conformation of SHP2 is in a closed state when not stimulated, with weakened phosphatase activity. However, upon stimulation from substances like epidermal growth factor (EGF), its closed conformation will open, activating the phosphatase activity and binding to the corresponding phosphorylated protein to act as a phosphatase. In the overall reaction, C-SH2 provides binding energy and specificity, but it does not have a direct role in activation.¹³ It has been proved that the change in the SHP2 phosphatase activity is closely associated with the disease. However, no study is available on the effect of SHP2 on IRI. Therefore, in this study, *in vivo* and *in vitro* assays were designed to investigate the effects of specific knockout of SHP2 in mononuclear macrophages on renal IRI and its molecular mechanisms.

RESULTS

Specific knockout of SHP2 could alleviate renal IRI

First, RT-PCR was performed to detect the SHP2 expression in the SHP2^{WT} group and the SHP2^{MAC-KO} group. The results showed that the expression of SHP2 in the SHP2^{MAC-KO} group was significantly lower than that in the SHP2^{WT} group (<). Moreover, the ultrasound VI value in the SHP2^{MAC-KO} group was significantly lower than that in the SHP2^{WT} group, and there was a significant difference between the two groups. The results of ELISA showed that the concentrations of BUN, Crea, and UA in the SHP2^{MAC-KO} group significantly decreased compared with the SHP2^{WT} group (Figure 1).

It was observed by Masson staining that the SHP2^{MAC-KO} group had milder interstitial edema and inflammatory cell infiltration, less necrotic and exfoliated cells in the renal tubules, and less swelling and degeneration of renal tubular epithelial cells than the SHP2^{WT} group. The result of immunofluorescence staining revealed that the relative fluorescence intensity of α -SMA, COL1, COL3, and Vim in the SHP2^{MAC-KO} group was significantly lower than that in the SHP2^{WT} group (Figure 2). All these results suggest that specific knockout of SHP2 can alleviate renal IRI and fibrosis.

Specific knockout of SHP2 could promote M2 polarization and inhibit M1 polarization

Flow cytometry results showed that compared with the SHP2^{WT} group, the M1 macrophages in the SHP2^{MAC-KO} group were significantly reduced, and the M2 macrophages were significantly increased. It was found by western blotting that compared with the SHP2^{WT} group, the relative protein expressions of TNF- α , IFN- γ , p-NF κ B, and p-MyD88 significantly decreased, while the relative protein expressions of Arginase-1, CD206, p-PI3K and p-I κ B significantly increased in the SHP2^{MAC-KO} group, displaying significant differences between the two groups (Figures 3 and 4). It can be seen that specific knockout of SHP2 can promote M2 polarization and inhibit M1 polarization.

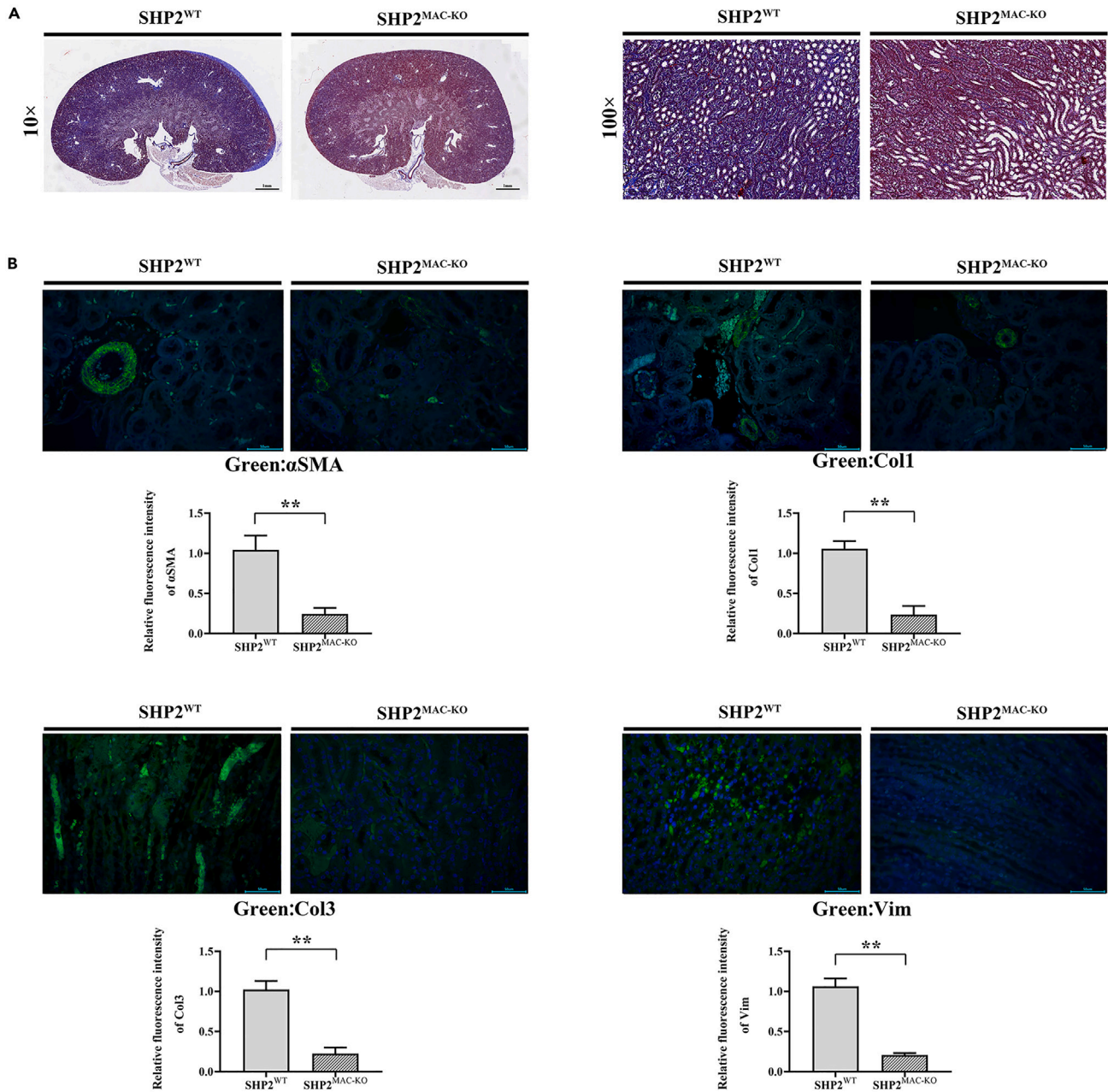


Figure 2. Renal pathological results of SHP2^{WT} group and SHP2^{MAC-KO} group

(A) Masson image of kidney in SHP2^{WT} group and SHP2^{MAC-KO} group; scale bar: 1 mm, scale bar: 100 μm.

(B) Immunofluorescence image of α-SMA, COL1, COL3, and Vim in SHP2^{WT} group and SHP2^{MAC-KO} group; scale bar: 50 μm; B: the relative fluorescence intensity of α-SMA, COL1, COL3, and Vim in SHP2^{WT} group and SHP2^{MAC-KO} group. N = 8; **p < 0.01.

Specific knockout of SHP2 could enhance the phagocytic ability of mononuclear macrophages

Compared with the SHP2^{WT} group, the SHP2^{MAC-KO} group had significantly increased relative expressions of p-PLCγ2, p-MerTK, and p-FAK, suggesting that specific knockout of SHP2 can increase the expression of endocytosis-related proteins (Figure 4).

In vitro specific knockout of SHP2 in macrophages could alleviate renal IRI

The result of western blotting showed that under normoxia, the relative protein expression of SHP2 in the SHP2^{MAC-KO} group was significantly lower than that in the SHP2^{WT} group, while there were no significant differences in p-PI3K, p-PLCγ2, p-MerTK, p-FAK, p-MyD88, TNF-α, IFNγ,

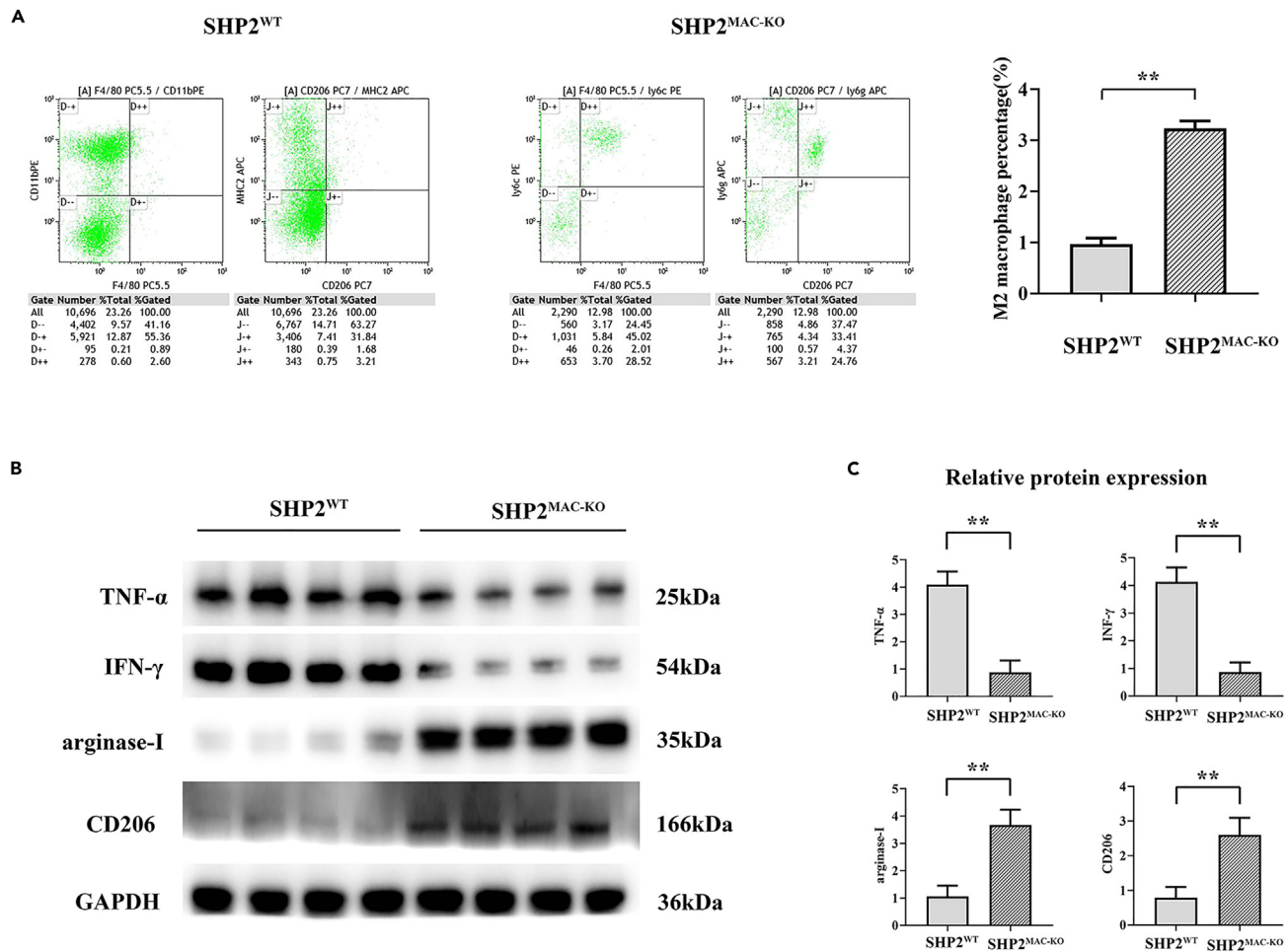


Figure 3. Specific knockout of SHP2 can promote M2 polarization and inhibit M1 polarization

(A) Flow cytometry for M2 macrophages was detected and the statistical results were obtained.

(B) Western blotting map of TNF- α , IFN γ , p-NF κ B, p-MyD88, arginase-1, CD206, p-PI3K, and p-I κ B in SHP2^{WT} group and SHP2^{MAC-KO} group.

(C) Statistics of relative protein expression of TNF- α , IFN γ , p-NF κ B, p-MyD88, arginase-1, CD206, p-PI3K, and p-I κ B in SHP2^{WT} group and SHP2^{MAC-KO} group. N = 8; **p < 0.01.

and p-NF κ B. Under hypoxia, the relative protein expressions of SHP2, p-MyD88, TNF- α , IFN- γ , and p-NF κ B significantly decreased, while the relative protein expressions of p-PI3K, p-PLC γ 2, p-MerTK, and p-FAK significantly increased in the SHP2^{MAC-KO} group compared with the SHP2^{WT} group. After the PI3K inhibitor LY294002 was added, the significant differences in the relative protein expressions of p-PI3K, p-PLC γ 2, p-MerTK, p-FAK, p-MyD88, and p-NF κ B were eliminated between the two groups. Besides, the results of phagocytosis assay showed that under normoxia, the number of fluorescent microspheres phagocytosed in the SHP2^{WT} group and SHP2^{MAC-KO} group was smaller without significant differences between the two groups. Under hypoxia, the number of fluorescent microspheres phagocytosed in the SHP2^{MAC-KO} group significantly increased compared with the SHP2^{WT} group, and the difference was eliminated after LY294002 was added. As observed by immunofluorescence staining, there was no significant difference in the relative fluorescence intensity of TNF- α and F-actin under normoxia between the two groups. Under hypoxia, the relative fluorescence intensity of TNF- α in the SHP2^{MAC-KO} group was significantly lower, while that of F-actin was significantly higher than those in the SHP2^{WT} group, but the differences were eliminated after LY294002 was added (Figures 5 and 6). All data are summarized in Table S1.

DISCUSSION

The pathophysiology of renal IRI appears to be heavily influenced by inflammation, which is a common abnormality. Inhibiting the inflammatory response is a therapeutic strategy for protecting the kidney tissues since IRI can trigger an inflammatory cascade that causes additional kidney damage. As major mediators of inflammation, chemokines can regulate the expression of pro-inflammatory cytokines,

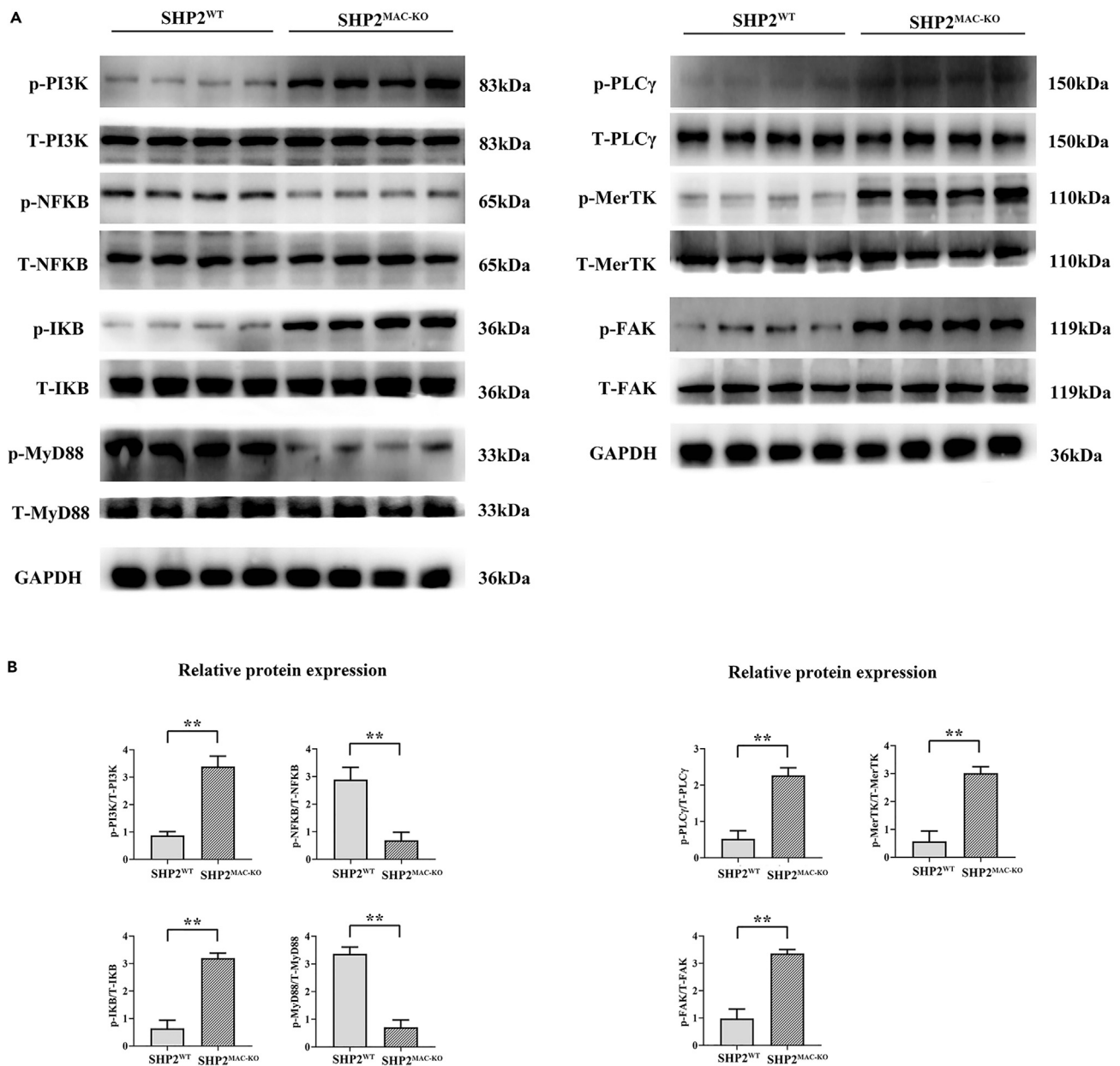


Figure 4. Specific knockout of SHP2 could promote monocyte macrophage endocytosis

(A) Western blotting map of p-PLC γ , p-MerTK, and p-FAK in SHP2^{WT} group and SHP2^{MAC-KO} group.

(B) Relative protein expression of p-PLC γ , p-MerTK, and p-FAK in SHP2^{WT} group and SHP2^{MAC-KO} group. N = 8; **p < 0.01.

adhesion molecules, and leukocyte infiltration and activation.^{15,16} Pro-inflammatory cytokines including IL-6 and TNF significantly contribute to renal IRI.

PI3K is a member of the phospholipase kinase family, which possesses double-enzymatic activity (lipid kinase and protein kinase). PI3K/Akt enables cells to respond to different stresses, particularly anti-apoptotic and pro-survival responses. Through the second messenger, PI3K can activate a variety of downstream protein kinases, such as Akt, of which phosphorylation is the key to activating the PI3K/Akt signaling pathway. Studies have shown that in IRI, PI3K/Akt is a classic protective signaling pathway.^{17,18} Moreover, the PI3K/Akt signaling pathway is an important way of exosome secretion, which can alleviate the hepatic IRI by targeting CRYAB. It can be inferred that the PI3K/Akt signaling pathway plays an important role in IRI.^{19,20} SHP2, a non-receptor protein tyrosine phosphatase encoded by the PTPN11 gene, has variable effects on the PI3K/Akt pathway: In at least some cell types, SHP2 negatively regulates epidermal growth factor (EGF)-evoked PI3K/Akt activation by dephosphorylating the PI3K binding site on GAB3.^{21–23} In this study, SHP2 was specifically

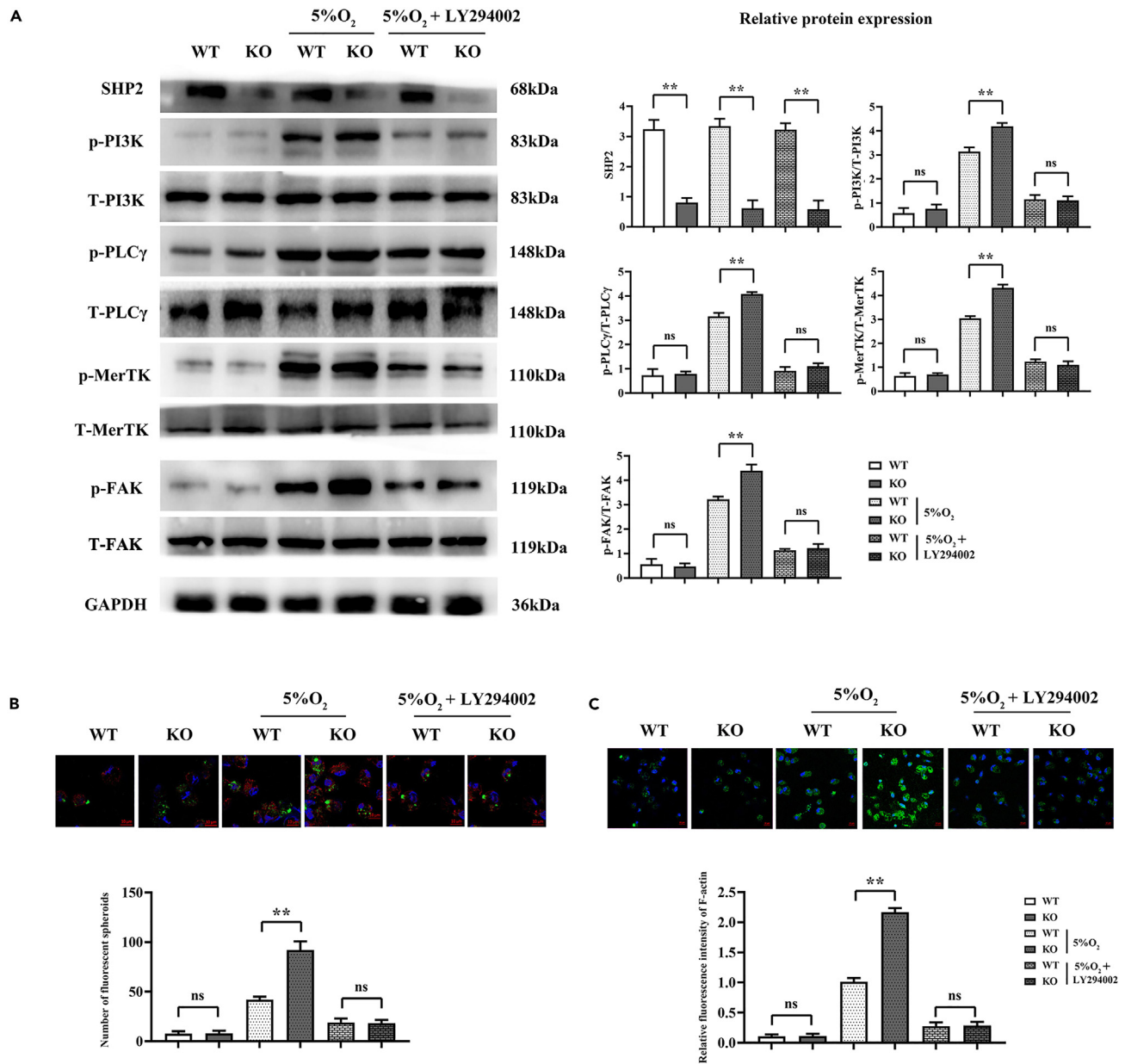


Figure 5. In vitro experiments verify that specific knockout of SHP2 can promote endocytosis of mononuclear macrophages

(A) Western blot results and statistics of relative protein expression of SHP2, p-PLC γ 2, p-MerTK, and p-FAK.

(B) Result of fluorescent microsphere phagocytosis experiment and statistics of phagocytosed fluorescent microsphere; scale bar : 10 μ m.

(C) F-actin immunofluorescence experiment results and statistics of relative fluorescence intensity. Scale bar : 10 μ m; N = 3; **p < 0.01; nsp > 0.05.

knocked out in mononuclear macrophages of C57BL/6 mice and then mouse renal IRI models were established. The ultrasound results showed that after specific knockout of SHP2, the ultrasound VI value significantly decreased. The interstitial edema and inflammatory cell infiltration were relieved, the number of necrotic and exfoliated cells in the renal tubules was reduced, the degree of swelling and degeneration of renal tubular epithelial cells was alleviated, and the relative fluorescence intensity of α -SMA, Col1, Col3, and Vim also significantly decreased. These findings suggest that specific knockout of SHP2 can alleviate renal IRI and fibrosis. Flow cytometry results showed that compared with the SHP2^{WT} group, the M1 macrophages in the SHP2^{MAC-KO} group were significantly reduced, and the M2 macrophages were significantly increased. Moreover, the results of western blotting showed that the relative protein expressions of TNF- α , IFN γ , p-NF κ B, and p-MyD88 in the SHP2^{MAC-KO} group were significantly lower than those in the SHP2^{WT} group, while the relative protein expressions of arginase-1, CD206, p-PI3K, p-PLC γ 2, p-MerTK, p-FAK, and p-I κ B were significantly higher than those in the

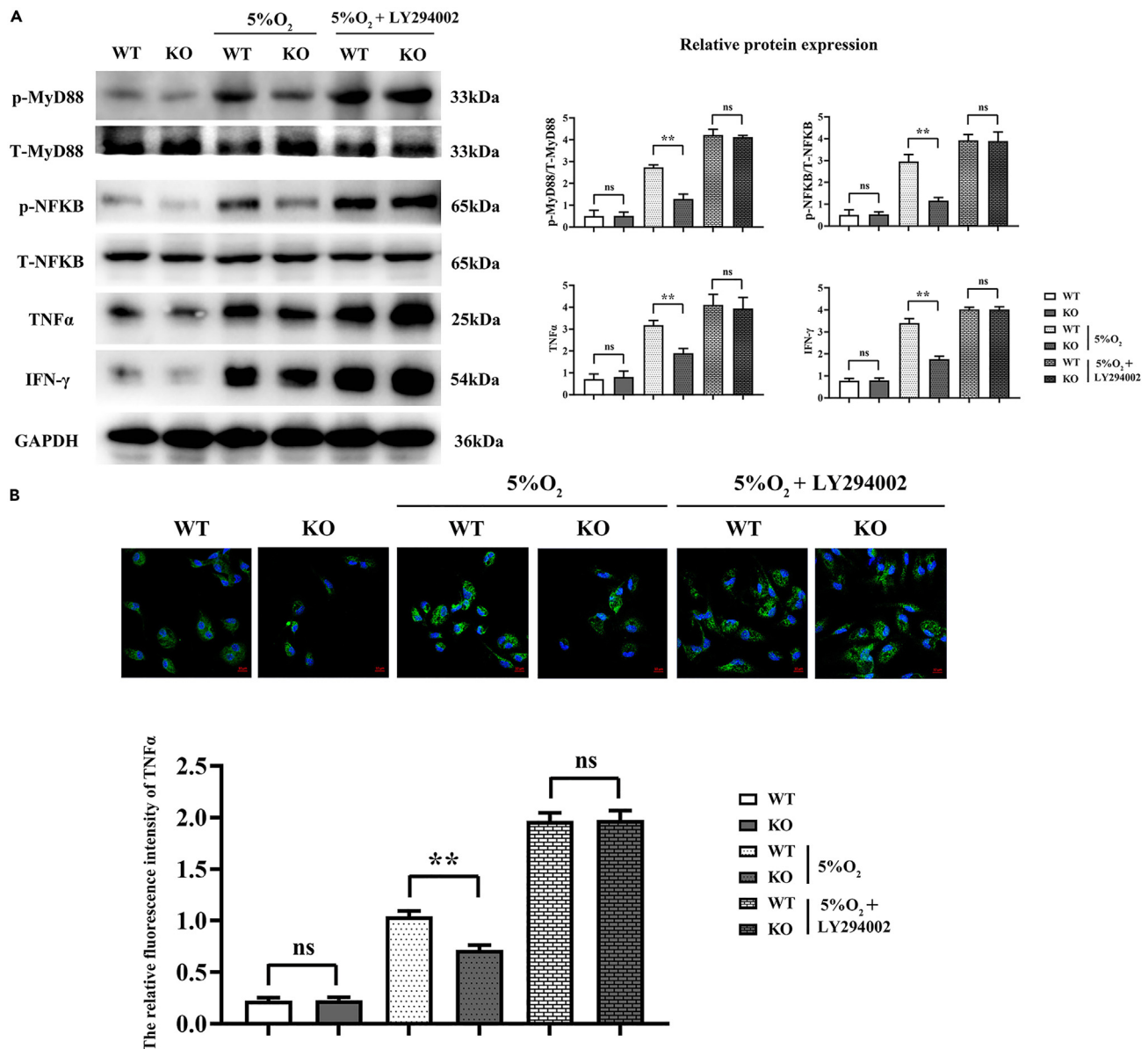


Figure 6. *In vitro* experiments verify that specific knockout of SHP2 can inhibit inflammatory response

(A) Western blot results of TNF- α , IFN γ , p-NF κ B, and p-MyD88 and statistics of their relative protein expressions.

(B) Immunofluorescence experiment results of TNF- α and statistics of relative fluorescence intensity. N = 3; **p < 0.01; nsp > 0.05.

SHP2^{WT} group, with significant differences. There is a relationship between macrophage polarization and IRI, i.e., the polarized state of macrophages may determine the severity of IRI and the tissue repair process. Overactivated M1 macrophages may increase the inflammatory response and thus further worsen tissue damage. In contrast, M2 macrophage polarization may help reduce inflammation and promote tissue repair. Studies have shown that inhibiting M1 macrophage polarization *in vivo* and *in vitro* can alleviate hepatic IRI.^{24–27} The results in this study showed that specific knockout of SHP2 could enhance M2 polarization and inhibit M1 polarization by activating the PI3K signaling pathway.

In the *in vitro* assay, mononuclear macrophages were cultured under normoxia, 5% O₂, and 5% O₂+LY294002, respectively. The result of western blotting showed that under normoxia, the relative protein expression of SHP2 in the SHP2^{MAC-KO} group was significantly lower than that in the SHP2^{WT} group, while there were no significant differences in p-PI3K, p-PLC γ 2, p-MerTK, p-FAK, p-MyD88, TNF- α , IFN γ , and p-NF κ B. Under hypoxia, the relative protein expressions of SHP2, p-MyD88, TNF- α , IFN- γ , and p-NF κ B significantly decreased, while the relative protein expressions of p-PI3K, p-PLC γ 2, p-MerTK, and p-FAK significantly increased in the SHP2^{MAC-KO}

group compared with the SHP2^{WT} group. After LY294002 was added, the significant differences in the relative protein expressions of p-PI3K, p-PLC γ 2, p-MerTK, p-FAK, p-MyD88, and p-NF κ B were eliminated between the two groups. Besides, the results of the phagocytosis assay showed that under normoxia, the number of fluorescent microspheres phagocytosed in the SHP2^{WT} group and SHP2^{MAC-KO} group was smaller without significant differences between the two groups. Under hypoxia, the number of fluorescent microspheres phagocytosed in the SHP2^{MAC-KO} group significantly increased compared with the SHP2^{WT} group, and the difference was eliminated after LY294002 was added.

Actin exists in two forms: G-actin (monomeric globular actin) and F-actin (polymeric filamentous actin), both of which are essential for cell movement and contractio.^{28–31} As observed by immunofluorescence staining in this study, there was no significant difference in the relative fluorescence intensity of TNF- α and F-actin under normoxia between the two groups. Under hypoxia, the relative fluorescence intensity of TNF- α in the SHP2^{MAC-KO} group was significantly lower, while that of F-actin was significantly higher than those in the SHP2^{WT} group, but the differences were eliminated after LY294002 was added.

In conclusion, specific knockout of SHP2 in mononuclear macrophages can promote M2 polarization and endocytosis, and inhibit M1 polarization and inflammatory response through the PI3K signaling pathway, thereby alleviating renal IRI.

Limitations of the study

In our model, all surviving mice, including control animals, returned to normal levels of renal function within 7 days of renal ischemia-reperfusion modeling with no significant long-term effects. Therefore, it is unclear whether our model generalizes the long-term sequelae of kidney injury that are common in human patients. Therefore, we need to conduct experimental studies on human renal ischemia-reperfusion related tissues in subsequent experiments.

STAR★METHODS

Detailed methods are provided in the online version of this paper and include the following:

- KEY RESOURCES TABLE
- RESOURCE AVAILABILITY
 - Lead contact
 - Materials availability
 - Data and code availability
- METHOD DETAILS
 - Experimental model and study participant details
 - Ethics approval
 - Modeling of renal IRI
 - Ultrasound testing of changes in renal structure and function
 - Masson staining
 - Immunofluorescence staining
 - Flow cytometry
 - Collection of bone marrow mesenchymal stem cells (BMMSCs)
 - RT-PCR
 - Enzyme-linked immunosorbent assay (ELISA)
 - Western blotting
 - Phagocytosis assay using fluorescent microspheres
- QUANTIFICATION AND STATISTICAL ANALYSIS

SUPPLEMENTAL INFORMATION

Supplemental information can be found online at <https://doi.org/10.1016/j.isci.2024.109048>.

ACKNOWLEDGMENTS

None.

Funding: None.

AUTHOR CONTRIBUTIONS

M.D.: Formal analysis, investigation, writing – original draft, and writing – review and editing. S.Z.: Conceptualization, methodology, and investigation. X.W.: Conceptualization and methodology. C.L.: Investigation. L.P.: Conceptualization and data curation. X.C.: Conceptualization and data curation. Y.Q.: Writing – review and editing, funding acquisition, project administration, resources, and supervision.

DECLARATION OF INTERESTS

The authors declare no competing interests.

Received: July 27, 2023

Revised: November 28, 2023

Accepted: January 23, 2024

Published: January 30, 2024

REFERENCES

- Zhao, H., Alam, A., Soo, A.P., George, A.J.T., and Ma, D. (2018). Ischemia-Reperfusion Injury Reduces Long Term Renal Graft Survival: Mechanism and Beyond. *EBioMedicine* 28, 31–42. <https://doi.org/10.1016/j.ebiom.2018.01.025>.
- Li, X., Ma, N., Xu, J., Zhang, Y., Yang, P., Su, X., Xing, Y., An, N., Yang, F., Zhang, G., et al. (2021). Targeting Ferroptosis: Pathological Mechanism and Treatment of Ischemia-Reperfusion Injury. *Oxid. Med. Cell. Longev.* 2021, 1587922. <https://doi.org/10.1155/2021/1587922>.
- Basile, D.P., Donohoe, D., Roethe, K., and Osborn, J.L. (2001). Renal ischemic injury results in permanent damage to peritubular capillaries and influences long-term function. *Am. J. Physiol. Ren. Physiol.* 281, F887–F899. <https://doi.org/10.1152/ajprenal.2001.281.5.F887>.
- Bos, E.M., Wang, R., Snijder, P.M., Boersema, M., Damman, J., Fu, M., Moser, J., Hillebrands, J.L., Ploeg, R.J., Yang, G., et al. (2013). Cystathionine γ -lyase protects against renal ischemia/reperfusion by modulating oxidative stress. *J. Am. Soc. Nephrol.* 24, 759–770. <https://doi.org/10.1681/asn.2012030268>.
- Bruno, S., Grange, C., Collino, F., Deregibus, M.C., Cantaluppi, V., Biancone, L., Tetta, C., and Camussi, G. (2012). Microvesicles derived from mesenchymal stem cells enhance survival in a lethal model of acute kidney injury. *PLoS One* 7, e33115. <https://doi.org/10.1371/journal.pone.0033115>.
- Lau, A., Rahn, J.J., Chappellaz, M., Chung, H., Benediktsson, H., Bihan, D., von Mässenhausen, A., Linkermann, A., Jenne, C.N., Robbins, S.M., et al. (2022). Dipeptidase-1 governs renal inflammation during ischemia reperfusion injury. *Sci. Adv.* 8, eabm0142. <https://doi.org/10.1126/sciadv.abm0142>.
- Dong, Y., Yin, J., Chen, T., Wen, J., Zhang, Q., Li, X., Lin, W., Liu, F., Fan, Y., and Wang, N. (2021). DL-3-n-butylphthalide pretreatment attenuates renal ischemia/reperfusion injury. *Biochem. Biophys. Res. Commun.* 557, 166–173. <https://doi.org/10.1016/j.bbrc.2021.04.006>.
- Shao, G., He, J., Meng, J., Ma, A., Geng, X., Zhang, S., Qiu, Z., Lin, D., Li, M., Zhou, H., et al. (2021). Ganoderic Acids Prevent Renal Ischemia Reperfusion Injury by Inhibiting Inflammation and Apoptosis. *Int. J. Mol. Sci.* 22, 10229. <https://doi.org/10.3390/ijms221910229>.
- Hasegawa, S., Inoue, T., Nakamura, Y., Fukaya, D., Uni, R., Wu, C.H., Fujii, R., Peerapanyasut, W., Taguchi, A., Kohro, T., et al. (2021). Activation of Sympathetic Signaling in Macrophages Blocks Systemic Inflammation and Protects against Renal Ischemia-Reperfusion Injury. *J. Am. Soc. Nephrol.* 32, 1599–1615. <https://doi.org/10.1681/asn.2020121723>.
- Liu, Z., Meng, Y., Miao, Y., Yu, L., Wei, Q., Li, Y., Zhang, B., and Yu, Q. (2021). Propofol ameliorates renal ischemia/reperfusion injury by enhancing macrophage M2 polarization through PPAR γ /STAT3 signaling. *Aging* 13, 15511–15522. <https://doi.org/10.18632/aging.203107>.
- Liu, C., Chen, K., Wang, H., Zhang, Y., Duan, X., Xue, Y., He, H., Huang, Y., Chen, Z., Ren, H., et al. (2020). Gastrin Attenuates Renal Ischemia/Reperfusion Injury by a PI3K/Akt/Bad-Mediated Anti-apoptosis Signaling. *Front. Pharmacol.* 11, 540479. <https://doi.org/10.3389/fphar.2020.540479>.
- Liu, H., Wang, L., Weng, X., Chen, H., Du, Y., Diao, C., Chen, Z., and Liu, X. (2019). Inhibition of Brd4 alleviates renal ischemia/reperfusion injury-induced apoptosis and endoplasmic reticulum stress by blocking FoxO4-mediated oxidative stress. *Redox Biol.* 24, 101195. <https://doi.org/10.1016/j.redox.2019.101195>.
- Zhu, G., Xie, J., Kong, W., Xie, J., Li, Y., Du, L., Zheng, Q., Sun, L., Guan, M., Li, H., et al. (2020). Phase Separation of Disease-Associated SHP2 Mutants Underlies MAPK Hyperactivation. *Cell* 183, 490–502.e18. <https://doi.org/10.1016/j.cell.2020.09.002>.
- Iadecola, C. (2013). The pathobiology of vascular dementia. *Neuron* 80, 844–866. <https://doi.org/10.1016/j.neuron.2013.10.008>.
- Shan, Y., Chen, D., Hu, B., Xu, G., Li, W., Jin, Y., Jin, X., Jin, X., and Jin, L. (2021). Allicin ameliorates renal ischemia/reperfusion injury via inhibition of oxidative stress and inflammation in rats. *Biomed. Pharmacother.* 142, 112077. <https://doi.org/10.1016/j.biopha.2021.112077>.
- Hou, J., Tolbert, E., Birkenbach, M., and Ghonem, N.S. (2021). Treprostinil alleviates hepatic mitochondrial injury during rat renal ischemia-reperfusion injury. *Biomed. Pharmacother.* 143, 112172. <https://doi.org/10.1016/j.biopha.2021.112172>.
- Liu, B., Deng, Q., Zhang, L., and Zhu, W. (2020). Nobiletin alleviates ischemia/reperfusion injury in the kidney by activating PI3K/AKT pathway. *Mol. Med. Rep.* 22, 4655–4662. <https://doi.org/10.3892/mmr.2020.11554>.
- El-Maadawy, W.H., Hassan, M., Hafiz, E., Badawy, M.H., Eldahshan, S., AbuSeada, A., El-Shazly, M.A.M., and Ghareeb, M.A. (2022). Co-treatment with Esculin and erythropoietin protects against renal ischemia-reperfusion injury via P2X7 receptor inhibition and PI3K/Akt activation. *Sci. Rep.* 12, 6239. <https://doi.org/10.1038/s41598-022-09970-8>.
- Li, J.H., Jia, J.J., He, N., Zhou, X.L., Qiao, Y.B., Xie, H.Y., Zhou, L., and Zheng, S.S. (2023). Exosome is involved in liver graft protection after remote ischemia reperfusion conditioning. *Hepatobiliary Pancreat. Dis. Int.* 22, 498–503. <https://doi.org/10.1016/j.hbpd.2022.04.004>.
- Huang, Z., Mou, T., Luo, Y., Pu, X., Pu, J., Wan, L., Gong, J., Yang, H., Liu, Y., Li, Z., et al. (2020). Inhibition of miR-450b-5p ameliorates hepatic ischemia/reperfusion injury via targeting CRYAB. *Cell Death Dis.* 11, 455. <https://doi.org/10.1038/s41419-020-2648-0>.
- Sun, Z., Liu, Q., Lv, Z., Li, J., Xu, X., Sun, H., Wang, M., Sun, K., Shi, T., Liu, Z., et al. (2022). Targeting macrophagic SHP2 for ameliorating osteoarthritis via TLR signaling. *Acta Pharm. Sin. B* 12, 3073–3084. <https://doi.org/10.1016/j.apsb.2022.02.010>.
- Heynen, G.J.J.E., Lisek, K., Vogel, R., Wulf-Goldenberg, A., Alcaniz, J., Montaudon, E., Marangoni, E., and Birchmeier, W. (2022). Targeting SHP2 phosphatase in breast cancer overcomes RTK-mediated resistance to PI3K inhibitors. *Breast Cancer Res.* 24, 23. <https://doi.org/10.1186/s13058-022-01521-3>.
- Kurupi, R., Floros, K.V., Jacob, S., Chawla, A.T., Cai, J., Hu, B., Puchalapalli, M., Coon, C.M., Khatri, R., Crowther, G.S., et al. (2022). Pharmacologic Inhibition of SHP2 Blocks Both PI3K and MEK Signaling in Low-epiregulin HNSCC via GAB1. *Cancer Res. Commun.* 2, 1061–1074. <https://doi.org/10.1158/2767-9764.crc-21-0137>.
- Bao, H.L., Chen, C.Z., Ren, C.Z., Sun, K.Y., Liu, H., Song, S.H., and Fu, Z.R. (2024). Polydatin ameliorates hepatic ischemia-reperfusion injury by modulating macrophage polarization. *Hepatobiliary Pancreat. Dis. Int.* 23, 25–34. <https://doi.org/10.1016/j.hbpd.2022.08.009>.
- Zou, Z., Shang, R., Zhou, L., Du, D., Yang, Y., Xie, Y., Li, Z., Zhao, M., Jiang, F., Zhang, L., and Zhou, P. (2023). The Novel MyD88 Inhibitor TJ-M2010-5 Protects Against Hepatic Ischemia-reperfusion Injury by Suppressing Pyroptosis in Mice. *Transplantation* 107, 392–404. <https://doi.org/10.1097/tp.0000000000004317>.
- Zhu, Y., Yang, L., Xu, J., Yang, X., Luan, P., Cui, Q., Zhang, P., Wang, F., Li, R., Ding, X., et al. (2020). Discovery of the anti-angiogenesis effect of eltrombopag in breast cancer through targeting of HuR protein. *Acta Pharm. Sin. B* 10, 1414–1425. <https://doi.org/10.1016/j.apsb.2020.02.007>.
- Zhang, Z., Gao, J., Yu, J., Zhang, N., Fu, Y., Jiang, X., Wang, X., Song, J., and Wen, Z. (2023). Transcriptome analysis of novel macrophage M1-related biomarkers and potential therapeutic agents in ischemia-reperfusion injury after lung transplantation based on the WGCNA and CIBERSORT algorithms. *Transpl. Immunol.* 79, 101860. <https://doi.org/10.1016/j.trim.2023.101860>.
- Dominguez, R., and Holmes, K.C. (2011). Actin structure and function. *Annu. Rev. Biophys.* 40, 169–186. <https://doi.org/10.1146/annurev-biophys-042910-155359>.

29. Bisaria, A., Hayer, A., Garbett, D., Cohen, D., and Meyer, T. (2020). Membrane-proximal F-actin restricts local membrane protrusions and directs cell migration. *Science (New York, N.Y.)* 368, 1205–1210. <https://doi.org/10.1126/science.aay7794>.
30. Zuo, Y., d'Aigle, J., Chauhan, A., and Frost, J.A. (2020). Genetic deletion of the Rho GEF Net1 impairs mouse macrophage motility and actin cytoskeletal organization. *Small GTPases* 11, 293–300. <https://doi.org/10.1080/21541248.2017.1405772>.
31. Zuidsherwoude, M., Green, H.L.H., and Thomas, S.G. (2019). Formin proteins in megakaryocytes and platelets: regulation of actin and microtubule dynamics. *Platelets* 30, 23–30. <https://doi.org/10.1080/09537104.2018.1481937>.

STAR★METHODS

KEY RESOURCES TABLE

REAGENT or RESOURCE	SOURCE	IDENTIFIER
Antibodies		
Anti-SHP2 antibody	Abcam	Cat#ab17753; RRID:AB_443978
Anti-TNF- α antibody	Abcam	Cat#ab9635; RRID:AB_2203950
Anti-IFN γ antibody	Abcam	Cat#ab178447; RRID:AB_2747844
Anti-Arginase-1 antibody	Abcam	Cat#ab91279; RRID:AB_10674215
Anti-CD206 antibody	BD Biosciences	Cat#551136; RRID:AB_394066
Anti-p-NF κ B antibody	Abcam	Cat#ab131493; RRID:AB_11159257
Anti-p-MyD88 antibody	Abcam	Cat#ab89576; RRID:AB_2282219
Anti-p-PLC γ antibody	Thermo Fisher Scientific	Cat#PA5-35465; RRID:AB_2552775
Anti-p-MerTK antibody	Abcam	Cat#ab14921; RRID:AB_2250636
Anti-p-FAK antibody	Abcam	Cat#ab4815; RRID:AB_304651
Anti-p-PI3K antibody	Huabio	Cat#HA721673; RRID:AB_3072786
Anti-p-I κ B antibody	Abcam	Cat#abab75907; RRID:AB_1310355
Anti-t-NF κ B antibody	Abcam	Cat#ab131546; RRID:AB_11156880
Anti-t-MyD88 antibody	Abcam	Cat#ab2064; RRID:AB_302807
Anti-t-PLC γ antibody	Bioworld Technology	Cat#BS1787; RRID:AB_1662086
Anti-t-FAK antibody	Abcam	Cat#ab33113; RRID:AB_732297
Anti-t-PI3K antibody	Novus	Cat#NB110-57347; RRID:AB_844161
Anti-t-I κ B antibody	Abcam	Cat#ab58331; RRID:AB_943786
Anti-t-MerTK antibody	Abcam	Cat#ab52968; RRID:AB_2143584
Anti-GAPDH antibody	Abcam	Cat#ab77514; RRID:AB_2232066
Chemicals		
sodium pentobarbital	Sigma Aldrich	P3761
Regaud's iron-hematoxylin	Solarbio	G4480
donkey serum	Sigma Aldrich	D9663
collagenase type IV	Solarbio	No. C8160
trypsin	Solarbio	No. T1350
SYBR Green qPCR Master Mix	Takara Biotechnology	cat. No. RR820A
Critical commercial assays		
PrimeScript RT Reagent Kit	Takara Biotechnology	No. RR036A
Experimental models: Cell lines		
bone marrow mesenchymal stem cells	Wuhan Prosa Life Science and Technology Co., Ltd	N/A
Experimental models: Organisms/strains		
SHP-2 knockout mice and wild-type mice	Henan Scebis Biotechnology Co., Ltd	N/A
Oligonucleotides		
Primers for qRT-PCR	This paper	N/A
Software and algorithms		
GraphPad Prism 8	GraphPad	N/A
SPSS 19.0	IBM	N/A

RESOURCE AVAILABILITY

Lead contact

The relevant experimental reagents, experimental methods, and related data of this study can be obtained by contacting Yinghui Qi (Shali8416@163.com).

Materials availability

The study did not generate new unique reagents.

Data and code availability

- The dataset is public and is the release date of the software.
- No original code was reported in this study.
- Any additional information needed to reanalyze the data reported in this article is available upon request from the primary contact.

METHOD DETAILS

Experimental model and study participant details

Using the Cre-loxP system, mononuclear macrophage-specific SHP-2-knockout mice (SHP-2^{MAC-KO}) and wild-type mice (SHP-2^{WT}) were selected from the offspring of SHP^{fl_{ox}/fl_{ox}}+C57BL/6 mice crossed. The animals were raised in the SPF animal room with a 12/12-h light/dark cycle. The usage of the animal room and all experimental procedures had been approved by the Animal Ethics Committee of Pudan Hospital, Pudong New Area, Shanghai and conformed to the animal welfare guidelines of the National Animal Experiment Committee. Moreover, the animals were given the greatest care. The ethics number is 20204Y0156.

Ethics approval

All animal experiments comply with the ARRIVE guidelines. This study was conducted in accordance with the Declaration of Helsinki and was approved by Experimental Animal Ethics Committee of.

Modeling of renal IRI

The mice were anesthetized by intraperitoneal injection of sodium pentobarbital (50 mg/kg). Then the limbs were fixed in a prone position on the mouse plate, and the tail vein was punctured with a 4-gauge needle. After hair removal from the back, one side of the back was cut open to isolate the kidney, and the renal pedicle was clamped with non-invasive artery clamps, resulting in 30 min of renal ischemia followed by reperfusion. In this way, the renal IRI model was established.

Ultrasound testing of changes in renal structure and function

All mice were subjected to ultrasound imaging examination. After the animal model was established, the tail vein was injected with 5×10^6 microbubbles and simultaneously subjected to ultrasound irradiation for 5 min using a planar non-focused ultrasound transmitter with a diameter of 2.2 cm and an area of 3.8 cm. The probe emission frequency was set as 1 MHz, and the sound pressure at 73.9 kPa. Ultrasound contrast imaging was performed using Philips IU22 color Doppler ultrasound diagnostic instrument and L9-3 high-frequency linear array probe. Then the images were observed by using coherent pulse sequence imaging technology, with a probe emission frequency of 7.0 MHz and a mechanical index (MI) of 0.18. After the first frame of the image was acquired, continuous ultrasound at high MI was emitted for 2-3 s to destroy the microbubbles. Five frames of the background image were further stored, and all contrast-enhanced images were stored on a CD for offline analysis.

Masson staining

The paraffin-embedded sections were placed in distilled water, stained with Regaud's iron-hematoxylin for 10 min, and washed thoroughly. Next, the sections were soaked with Ponceau acid fuchsin staining solution for 10 min and with 2% glacial acetic acid solution for 1 min. Then, they were differentiated with 1% phosphomolybdic acid solution for 3 min, stained with Water blue or light green solution for 5 min, and soaked with 2% glacial acetic acid solution for 1 min. Afterward, the sections were dehydrated with 95% ethanol three times (10 s each time), transparentized with xylene three times (1 min each time), and mounted with neutral gum.

Immunofluorescence staining

The kidney tissues and mononuclear macrophages were fixed with 4% paraformaldehyde, Permeabilize with 0.1% Triton X-100 for 10 min, and then wash 3 times with PBS for 5 min each time, and blocked in 10% donkey serum (Sigma Aldrich). Then the cells were incubated overnight with the primary antibodies, and incubated with the secondary antibodies the next day. Finally, the images were captured using a fluorescence microscope (Leica, $\times 400$).

Flow cytometry

The kidney tissues were harvested under aseptic conditions, and cut into 1 mm tissue blocks with aseptic scissors. Then the tissue blocks were digested with a mixture of 0.2% collagenase type IV (Solarbio, article No. C8160) and 0.25% trypsin (Solarbio, article No. T1350) at 37°C. The mixture was stirred in a 50 mL Erlenmeyer flask using a sterile miniaturized magnetic stir bar on a mixer several times (5 min each time) until the tissue blocks disappeared. After the digestion was terminated with a complete medium, the supernatant was collected and filtered with a 200-mesh sieve to obtain the cell suspension. The cells were resuspended with PBS buffer containing 1% BSA and stored at 4°C for later use. After adjusting the cell density to $1 \times 10^6/100 \mu\text{L}$, F4/80 (Invitrogen, 11-4801-82) and CD206 (Invitrogen, 17-2061-82) were added, and stain in the dark for 30 min, and sorted by BD FACSAria III.

Collection of bone marrow mesenchymal stem cells (BMMSCs)

The tibia, femur, and iliac bones of mice were isolated, and the cells from the bone marrow were collected using a syringe containing DMEM. The bone marrow cells were cultured in DMEM supplemented with 10 ng/mL M-CSF and 10% fetal bovine serum (FBS) for 7 days to obtain BMMSCs. Then BMMSCs were cultured in DMEM with 10% FBS and 1% penicillin-streptomycin solution in a tri-gas incubator with 5% O₂ at 37°C, and then treated with 25 μM LY294002 (a PI3K inhibitor).¹⁴

RT-PCR

Total RNA was isolated using TRIzol reagent and synthesized into cDNA using the PrimeScript RT Reagent Kit (article No. RR036A; Takara Biotechnology) according to the manufacturer's instructions. Then qPCR was performed using the SYBR Green qPCR Master Mix (article No. RR820A; Takara Biotechnology) according to the manufacturer's instructions under the following conditions: Denaturation at 95°C for 30 s, followed by 40 cycles at 95°C for 5 s, 55°C for 30 s and 72°C for 30 s, and 1 cycle at 95°C for 60 s, 55°C for 30 s and 95°C for 30 s. Each sample had three replicates. The target gene expression was normalized to the expression of GAPDH, and the differential gene expression was calculated using the $2^{-\Delta\Delta C_t}$ method. The primer sequences used were as follows: SHP2 F: 5'-CCGCAGATTCAGGGATTACT-3', R: 5'-CTTGAAACGGACCAGTTC-3'.

Enzyme-linked immunosorbent assay (ELISA)

The blood sample was collected into anticoagulant tubes and centrifuged. Then the concentrations of blood urea nitrogen (BUN), creatinine (Crea) and uric acid (UA) were measured using ELISA kits according to the manufacturer's instructions. To be specific, the antigen was coated onto an ELISA plate (100 μL per well) and incubated at 37°C for 4 h before the liquid was discarded. Then the sample was blocked with 5% calf serum at 37°C for 40 min, washed 3 times, and added into reaction wells (100 μL per well) at 37°C for 40–60 min, followed by incubation with antibodies at 37°C for 60 min. After washing 3 times, chromogenic substrate (TMB) was added. Finally, the OD value was measured at a wavelength of 450 nm with a microplate reader, based on which the concentrations of BUN, Crea, and UA were detected.

Western blotting

The cells were digested with trypsin, washed with PBS and centrifuged. After the supernatant was discarded, the cells were fully lysed with an appropriate amount of RIPA lysis buffer to extract the total protein. The protein concentration was quantified by the BCA assay, and the buffer was boiled in a metal bath for 10 min. Then the protein sample (20 μg /well) was separated by SDS-PAGE, transferred onto a PVDF membrane, sealed with 5% skimmed milk powder for 2 h at room temperature, and incubated with primary antibodies against SHP2 (Abcam, ab17753, 1:1000), TNF- α (Abcam, ab9635, 1:1000), IFN γ (Abcam, ab178447, 1:1000), Arginase-1 (Abcam, ab91279, 1:1000), CD206 (BD Biosciences, 551136, 1:1000), p-NF κ B (Abcam, ab131493, 1:1000), p-MyD88 (Abcam, ab89576, 1:1000), p-PLC γ (Thermo Fisher Scientific, BS1787, 1:2000), p-MerTK (Abcam, ab14921, 1:1000), p-FAK (Abcam, ab4815, 1:1000), p-PI3K (Huabio, HA721673, 1:1000), p-I κ B (Abcam, ab75907, 1:1000), t-NF κ B (Abcam, ab131546, 1:1000), t-MyD88 (Abcam, ab2064, 1:1000), t-PLC γ (Bioworld Technology, BS1787, 1:2000), t-MerTK (Abcam, ab52968, 1:1000), t-FAK (Abcam, ab33113, 1:1000), t-PI3K (Novus, NB110-57347, 1:1000), t-I κ B (Abcam, ab58331, 1:1000) and GAPDH (Abcam, ab77514, 1:10000) overnight at 4°C. The next day, the membrane was washed with TBST, and incubated with HRP-labeled secondary antibodies (Abcam, ab205718, 1:10000) at room temperature for 2 h. After washing with TBST, the membrane was added with ECL solution and exposed in the gel imaging system. Finally, the gray value was analyzed.

Phagocytosis assay using fluorescent microspheres

The cells were starved and incubated on glass slides with 10 μm fluorescent silver YG microsphere latex beads (Polysciences; 4.55×10^6 beads/mL) for 24 h. Then the slides were washed thoroughly with PBS, fixed with 4% paraformaldehyde, and stained with 4',6-diamidino-2-phenylindole (for nuclei) and 1,1'-octacosyl-3,3,3',3'-tetramethylindoline (for membranes) in accordance with the manufacturer's instructions (Molecular Probes). Then they were inverted and mounted with Vectorshield antifade mounting medium. The fluorescence of latex beads, 4',6-diamidino-2-phenylindole, and 1,1'-octacosyl-3,3,3',3'-tetramethylindoline was activated using different excitation lights, and digital images were captured under a fluorescence microscope. To quantitatively determine the uptake of latex beads by cells, the number of beads was counted in several fields of view under different experimental conditions.

QUANTIFICATION AND STATISTICAL ANALYSIS

SPSS25.0 and Prism 8.0 software were used for data and image analysis. Enumeration data were described by ($\chi \pm s$), and t-test was performed on normally distributed data. Measurement data were described by median or interquartile range, and chi-square test was performed. $p < 0.05$ was considered statistically significant.